Chapitre II : Caractérisation d'une choroïde reconstruite par génie tissulaire

Research article

Characterization of a tissue-engineered choroid.

Aïcha Dede Djigo, Julie Bérubé, Solange Landreville et Stéphanie Proulx.

En préparation pour soumission au journal *Acta Biomateriala*.

2.1 Résumé

La choroïde de l'œil est un tissu conjonctif vascularisé et pigmenté localisé entre la rétine et la sclère. Il apparait de plus en plus que, en plus d'assurer la nutrition de la rétine externe, les différentes cellules choroïdiennes contribuent à l'homéostasie de la rétine, et ce particulièrement par la signalisation paracrine. Le rôle précis de chaque type cellulaire n'est cependant pas bien connu. Dans cette étude, nous avons développé un substitut choroïdien en utilisant l'approche de l'auto-assemblage du génie tissulaire. Nous avons isolé et cultivé les cellules de l'épithélium pigmentaire rétinien (EPR), les fibroblastes du stroma choroïdien, les cellules endothéliales vasculaires choroïdiennes et les mélanocytes choroïdiens, et ce à partir de tissus humains. Les fibroblastes ont été cultivés dans un milieu contenant du sérum et de l'acide ascorbique. Après 6 semaines, les cellules ont formé des feuillets de matrice extracellulaire (MEC) que nous avons empilé afin de former un substitut choroïdien reconstruit (SCR). Ce dernier a par la suite été caractérisé et comparé à la choroïde native. Leur composition de la MEC (collagènes et protéoglycanes) et leurs propriétés biomécaniques (résistance maximale à la traction, déformation et élasticité) étaient similaires. De plus, les cellules de l'EPR, les cellules endothéliales de la veine ombilicale humaine et les mélanocytes choroïdiens ont recolonisé avec succès les SCR. Il y a eu formation de structures physiologiques telles qu'une monocouche confluente de cellules de l'EPR, des structures de type capillaires, ainsi qu'une repigmentation. Nos SCR ont en conséquent mimé l'environnement biophysique de la choroïde native et peuvent servir de modèles pour l'étude des interactions normales entre l'EPR et les cellules choroïdiennes, de même que leurs échanges réciproques avec la MEC. Cela représente une première étape pouvant guider l'étude des mécanismes menant aux maladies affectant la choroïde.

2.2 Abstract

The choroid of the eye is a vascularized and pigmented connective tissue that lies between the retina and the sclera. Increasing evidence demonstrates that, beyond supplying nutrients to the outer retina, the different choroidal cells contribute to the retina's homeostasis, especially by paracrine signaling. However, the precise role of each cell type is currently unclear. Here, we developed a choroidal substitute using the self-assembly approach of tissue engineering. Human tissues were used to isolate and culture retinal pigment epithelial cells (RPE), choroidal stromal fibroblasts, choroidal vascular endothelial cells and choroidal melanocytes. Fibroblasts were cultured in a growth medium containing serum and ascorbic acid. After six weeks, cells formed sheets of extracellular matrix (ECM) that were stacked to produce a tissue-engineered (TE) choroidal substitute. This engineered stroma was then characterized and compared to the native choroid. Their ECM composition (collagens and proteoglycans) and biomechanical properties (ultimate tensile strength, strain and elasticity) were similar. Furthermore, RPE cells, human umbilical vein endothelial cells and choroidal melanocytes successfully repopulated the TE stromas. Physiological structures were established, such as a confluent monolayer of RPE cells, capillary-like structures, and a repigmentation. Our TE choroidal substitute thus recaptured the biophysical environment of the native choroid, and can serve as study models to understand the normal interactions between the RPE and choroidal cells, as well as their reciprocal exchanges with the ECM. This will consequently pave the way to derive accurate insight in the pathophysiological mechanisms of diseases affecting the choroid.

2.3 Introduction

The choroid is the posterior part of the middle vascular coat of the eye and is located between the sclera and the retinal pigment epithelium (RPE). It is mainly composed of blood vessels surrounded by a connective tissue containing collagen, elastic fibers and other extracellular matrix (ECM) components. Embedded in the loose choroidal stroma are fibroblasts, numerous melanocytes giving the tissue its dark pigmentation, smooth muscle and immune cells as well as nerves [1]. RPE and photoreceptor cells are dependent on the choroid for nutrients and oxygen supply along with waste removal [1], while the vascular endothelial growth factor (VEGF) secreted by the RPE mediates choroidal vascular endothelial cell (CVEC) survival and maintains choriocapillaris (CC) fenestrations [2].

Defects in the mutualistic symbiotic relationship between RPE cells and CC are implicated in age-related macular degeneration (AMD), a multifactorial, chronic and evolutive disease in which central vision is severely compromised or lost [3]. AMD affects more than 8% of the population worldwide, particularly those living in industrialized countries [4]. Blindness occurs either after an atrophy of the RPE and overlying photoreceptors (called dry AMD) or the invasion of the RPE and/or retina by choroidal neovessels (called wet AMD) in the macula [5]. In dry AMD, the degeneration of CC is secondary to the RPE loss due to the accumulation of toxic substances in the cells. However, in wet AMD, CC become dysfunctional in the proinflammatory environment of the choroid/retina, making the RPE cells hypoxic, thus leading to the production of angiogenic factors [3]. Alternatively, the increased secretion of VEGF could originate from the breakdown of the outer blood-retina barrier maintained by the RPE and the subsequent recruitment of circulating macrophages [6].

The choroid has long been considered only in relation to its functions associated with vascularization. However, it is becoming increasingly evident that choroidal cells synthetize growth factors and enzymes that can potentially affect neighboring cells of the sclera and the retina, in addition to playing a role in the normal development and regulation of the tissue [1, 7]. The function of choroidal melanocytes (CM), besides providing pigmentation, is still not fully elucidated though it is suggested that they mitigate oxidative

damages to the choroid/RPE, namely by quenching reactive oxygen species [8-10]. The modifications of the expression of matrix metalloproteases by choroidal cells may also play a role in drusen formation [11]. In addition, angiocrine factors released by CVEC have recently been implicated in the regulation of the RPE tight junctions and thus the outer blood-retina barrier [12]. Thus, there is much that could be learned by studying the normal interactions of choroidal cells with their ECM.

Tissue culture can help investigate the normal physiology of choroidal cells. However, 2D-cultured cells modify their structural and functional behaviors since they are deprived of their natural 3D environment, and are thus less physiologically relevant [13]. Indeed, the ECM provides signals for many cellular functions including cell growth, differentiation and migration, while its biomechanical and physical properties, notably its elasticity, can also influence cell behaviors via the phenomenon of mechanotransduction [13, 14].

As a result, the use of 3D biomimetic models is being more and more embraced especially in cancer research and drug development owing to the realistic and controllable environment they provide [15]. Various synthetic, natural or hybrid scaffolds and matrices, into which cells are seeded, have been used to establish 3D models. One method to produce these models without exogenous biomaterials consist in the self-assembly approach. Cornea [16, 17], skin [18], blood vessels [19, 20], as well as bone tissue [21], adipose tissue [22] and urological tissues [23, 24] have previously been engineered by taking advantage of the capacity of mesenchymal cells to secrete and "self-assemble" their own ECM proteins following the addition of ascorbic acid in the culture medium. Ascorbic acid stimulates the secretion of several ECM components, notably of collagen, thus leading to the production of a matrix sheet [19, 25]. These substitutes share similar ECM composition and biomechanical properties with their native tissues and are currently being used as study models and/or for transplantation purposes.

In this study, we demonstrate for the first time that it is possible to engineer choroidal stromas using the self-assembly approach. Using the principle of "deconstruction-reconstruction", fibroblasts, CVEC and melanocytes were first isolated from human

choroids, in addition to the RPE monolayer, and their purity was assessed. The main objectives were to compare the contractility, ECM composition, thickness, and biomechanical properties of tissue-engineered (TE) stromas produced by choroidal stromal fibroblasts (CSF) to the native tissue, as well as their biocompatibility for the seeding of RPE, vascular endothelial cells and choroidal melanocytes (CM).

2. 4 Material and methods

2.4.1 Human eyes

The study followed the tenets of the Declaration of Helsinki, and was approved by the CHU de Québec-Université Laval institutional human experimentation committee (Quebec City, Canada). Fifteen human eyes from fifteen donors were provided by our local Eye Bank (Banque d'Yeux du Centre Universitaire d'Ophtalmologie, Quebec City, Quebec, Canada). Written informed consent for research purposes was obtained from the donor's next-of-kin. Donor age ranged from 54 to 86 years old (8 women, 7 men) and eyes were processed within three days. No information was available concerning the medical history of the donated eyes. However, there were no overt signs of ophthalmic diseases during the macroscopic examination of the dissected choroid or the histopathological analysis of cross sections (such as the presence of confluent drusen, hypopigmentation of the RPE or exudates/hemorrhages).

2.4.2 Isolation and culture of human RPE and choroidal cells

2.4.2.1 Dissection

Under sterile conditions, the eyeballs were opened below the ora serrata and the anterior segment, vitreous, and neural retina were discarded. Phosphate-buffered saline (PBS: 137 mM NaCl, 2.7 mM KCl, 6.5 mM Na2HPO4, pH 7.4) was added into the eyeball and the remaining neural retina still attached to the optic nerve head was removed by gentle pipetting. The eyeball was then cut into a four-petal shape and rinsed with PBS. The RPE/choroid complex was subsequently delicately peeled off the sclera and treated for 30 to 60 min with 0.02% EDTA (Sigma-Aldrich, Ontario, Canada) or 2 U/ml dispase solution (Roche, Indianapolis, USA) at 37˚C. Ten globes from ten donors were used to isolate the RPE and choroidal cells.

2.4.2.2 RPE isolation and culture

Small RPE sheets were dislodged from the choroid by repeatedly pipetting up and down the EDTA/dispase solution. RPE cells were transferred in a 15 ml tube, rinsed, and cultured in Dulbecco–Vogt modified Eagle medium (DMEM; Corning, Ontario, Canada) supplemented with 10% fetal bovine serum (FBS; Seradigm, Utah, USA) and 100 U/mL penicillin – 100 µg/mL streptomycin (P/S) (Corning).

2.4.2.3 Choroidal vascular endothelial cell (CVEC) isolation and culture

Remaining RPE cells were washed away by vigorous pipetting. Choroids were then incubated overnight in 0.125 U/ml collagenase H (Roche) at 37°C, with frequent agitation. This digested tissue mixture was centrifuged, and resuspended in trypsin-EDTA (Corning) for 10 minutes at 37˚C, then the enzymatic digestion was neutralized in DMEM supplemented with 10% FBS, and filtered with a 40 µm cell strainer (Corning). CVEC were extracted from this dissociated cell suspension using Dynabeads® CD31 in PBS/0.5% BSA/2 mM EDTA according to the manufacturer's instructions (Invitrogen, Oslo, Norway). Purified CVEC were resuspended in the endothelial growth medium EGM-2 (EBM-2 basal medium and EGM-2 MV SingleQuot Kit Suppl. & Growth Factors; Lonza, Ontario, Canada), and seeded on 0.5% gelatin-coated flasks.

2.4.2.4 Choroidal stromal fibroblast (CSF) isolation and culture

Washing fractions collected during the CVEC isolation (containing CSF and CM) were pooled and centrifuged. Cells were resuspended in DMEM 10% FBS and split in half. One half was used to culture choroidal fibroblasts in DMEM supplemented with 10% FBS and P/S. After two passages, the fibroblasts outgrew the other choroidal cells (namely the CM).

2.2.4.5 Choroidal melanocyte (CM) isolation and culture

The remaining half of the cell solution was centrifuged again and cells were resuspended in a melanocyte selection medium containing (1:1) DMEM (Corning)/Ham's F12 medium (Wisent, Quebec, Canada) supplemented with 10% FBS, 10 ng/ml cholera toxin (Sigma), 100 nM phorbol 12-myristate 13-acetate (Sigma), 50 µg/ml gentamicin (Thermo Fisher Scientific, Ontario, Canada), and 100 µg/ml geneticin (Sigma). Geneticin is a selective cytotoxic agent that eliminates rapidly proliferating cells such as fibroblasts.

2.2.4.6 Purity assessment of cell cultures

2.2.4.6.1 Immunolabeling

Cells were seeded on glass coverslips in their respective culture conditions, then fixed with 90% acetone for 10 min at -20˚C, and processed for immunofluorescent staining, as described in section 2.4.4.3. A panel of antibodies was used to determine the purity of RPE, CVEC, CSF and CM cultures (see Table 2.1). Anti-keratins 8/18, anti-VE-cadherin, anti-HMB-45 and anti-vimentin were used to identify RPE cells, vascular endothelial cells, melanocytes and fibroblasts, respectively.

Table 2.1 Primary and secondary antibodies used for immunofluorescent stainings.

Primary antibodies			
Epitope	**Clone**	**Host species**	**Source**
Collagen I	COL-1	Mouse, monoclonal	Sigma
Collagen III		Rabbit, polyclonal	CedarLane
Collagen IV		Rabbit, polyclonal	Abcam
Collagen V		Rabbit, polyclonal	CedarLane
Collagen VI		Rabbit, polyclonal	Abcam
Decorin	115402	Mouse, monoclonal	R&D Systems
Fibronectin		Goat, polyclonal	Santa Cruz Biotechnology
HMB45	HMB-45	Mouse, monoclonal	Dako
K8/K18	5D3	Mouse, monoclonal	Abcam
Lumican	EPR8898(2)	Mouse, monoclonal	Abcam
Perlecan	A7L6	Rat, monoclonal	Abcam
Tenascin C	EB2	Mouse, monoclonal	Abcam
VE-cadherin		Rabbit, polyclonal	Abcam
Vimentin	V9	Mouse, monoclonal	Abcam
α-SMA	1A4	Mouse, monoclonal	Abcam

Secondary antibodies	
Type	**Source**
Goat anti-mouse IgG H+L antibodies conjugated with Alexa 594	Invitrogen
Chicken anti-rabbit IgG H+L antibodies conjugated with Alexa 594	Invitrogen
Goat anti-rat IgG H+L antibodies conjugated with Alexa 594	Invitrogen
Chicken anti-goat IgG H+L antibodies conjugated with Alexa 594	Invitrogen

2.2.4.6.2 Gene expression profiling

Total RNA was isolated from CSF (n=3 populations) and from one population of RPE cells using the RNeasy Mini Kit (QIAGEN, Ontario, CA). The RNA quality was analyzed using the 2100 Bioanalyser (Agilent Technologies, Ontario, Canada). All samples had a RNA integrity number (RIN) of 10. Cyanine 3-CTP labeled cRNA targets were prepared from 50

ng of total RNA using the Agilent One-Color Micro-Array-Based Gene Expression Analysis kit (Agilent Technologies). The cRNA (600 ng) was incubated on a G4851A SurePrint G3 Human GE 8x60 K array slide (60,000 probes, Agilent Technologies), and the slides were hybridized and scanned on an Agilent SureScan Scanner according to the manufacturer's instructions. The data were then analyzed using the ArrayStar V12 (DNASTAR, Wisconsin, USA) software for scatter plots and for the generation of heatmaps for selected genes of interest. The raw data generated from the arrays were preprocessed using RMA (Robust Multiarray Analysis) for background correction. It was subsequently transformed in log2 base after quantile normalization before a linear model was fitted to the normalized data to obtain an expression measure for each probe set on the array. The color scale used in the heatmaps to display the log2 expression level values was determined by the Hierarchical clustering algorithm of the Euclidian metric distance between genes. The housekeeping mRNA golgin A1 (GOLGA1) and beta-2-microglobulin (B2M) were used as internal controls to normalize the linear signals of the selected mRNA of interest [26]. The microarray data presented in this study complied with the Minimum Information About a Microarray Experiment (MIAME) requirements [27].

2.4.3 Production of choroidal stromal substitutes using the self-assembly approach of tissue engineering

Passages 2 to 7 of CSF isolated from eight different donors were seeded in 6-well plates (Corning) with an anchoring paper ring. Cells were grown in DMEM supplemented with 10% FBS and 50 µg/ml ascorbic acid (Sigma, Missouri, USA). After six weeks of culture, the matrix sheets could be manipulated, and two sheets were thus stacked to form a thicker substitute. These TE choroidal stromal substitutes were kept in culture for one to two more weeks before their analysis.

2.4.4 Characterization of the tissue-engineered choroidal stromas

2.4.4.1 Contraction assays

To assess the contractility of TE stromas, a circular cut was made in the center of the substitutes using a 10-mm biopsy punch (Acuderm, Florida). Pictures were taken with a stereomicroscope (Zeiss SteREO Discovery.V8, Ontario, Canada) at 0, 1, 10, 30, 60 and 120 minutes. Experiments were performed in triplicates using 8 different cell populations.

The surface area of the released tissue at selected times was calculated using the ImageJ software, and the percentage of contractility was determined with the formula 100*(1- area at time point/initial area).

2.4.4.2 Mass spectrometry

The in-gel digest and mass spectrometry experiments were performed by the Proteomics platform of the Eastern Quebec Genomics Center (Quebec, Canada). Circular samples (2.4 cm width) were cut in half prior to solubilization in Laemmli buffer. The protein concentration was determined using colorimetric Bradford assay according to Bio-Rad instructions. Material was separated using a 4-12% gradient SDS-PAGE criterion gel (BioRad). The gel was then stained with SYPRO Ruby fluorescent protein stain (Bio-Rad) as per the manufacturer's instructions. Bands of interest were extracted from the gel and placed in 96-well plates and then washed with water. Tryptic digestion was performed on a MassPrep liquid handling robot (Waters, Milford, USA) according to the manufacturer's specifications and to the protocol of Shevchenko [28] with the modifications suggested by Havlis and collaborators [29]. Protein in-gel digestion and mass spectrometry were conducted as previously reported [17]. All MS/MS samples were analyzed using the Mascot software (Matrix Science, London, UK; version 2.3.0) set up to search the Uniref100 database Homo sapiens (release 11 05). Search parameters were as followed: fragment ion mass tolerance of 0.50 Da, parent ion tolerance of 2.0 Da, fixed modification of iodoacetamide derivative on cysteine, variable modification of oxidation on methionine, and 2 missed cleavage allowed. The Scaffold software (version 3.0.0), Proteome Software Inc., Oregon, USA) was used to validate MS/MS based peptide and protein identifications. Peptide identifications were accepted if they could be established at greater than 95.0% probability as specified by the Peptide Prophet algorithm [30]. Protein identifications were accepted if they could be established at greater than 95.0% probability and contained at least 2 identified peptides. Protein probabilities were assigned by the Protein Prophet algorithm [31]. Proteins that contained similar peptides and could not be differentiated based on MS/MS analysis alone were grouped to satisfy the principles of parsimony.

2.4.4.3 Immunofluorescent staining

TE choroidal stromal substitutes (N=8) were embedded in optimal cutting temperature (OCT) compound (Sakura Finetek, USA Inc.) and stored in liquid nitrogen until their use.

Five to 10 µm-thick cryosections were cut using a cryostat (Leica, Concord, Canada), air-dried, fixed in acetone for 10 minutes at -20°C and rinsed with PBS-IF (PBS supplemented with 0.9 mM CaCl2, 0.48 mM MgCl2) containing 1% BSA. Slides were washed three times with PBS-IF, incubated with primary antibodies at room temperature for 45 min, washed three times with PBS-IF, and then incubated 30 min in the dark with their respective secondary antibody. Cell nuclei were counterstained using Hoechst reagent 33258 (Sigma). Imaging was carried out using a Zeiss Axio Imager.Z2 microscope (Carl Zeiss, Ontario, Canada). Negligible background was observed for negative controls (primary antibodies were omitted). Table 2.1 describes the source of the different antibodies used for the detection of collagen types I, III, IV, V and VI, decorin, lumican, perlecan, α-SMA, smoothelin, fibronectin and tenascin C. These immunostainings were also performed on native human tissues (4 eyeballs from 4 donors).

2.4.4.4 Scanning electron microscopy

TE choroidal stromal substitutes (N=3) were fixed with 3.7% formaldehyde (ACP Chemicals, Québec, Canada), dehydrated with ethanol and ethyldisilazane solutions, and then sputtered with gold palladium particles using a gold-coated sputter (EMS, Cedarlane, Ontario, Canada). Images were taken with a Jeol 6460LV (Tokyo, Japan) scanning electron microscope (IBIS microscopy platform, Université Laval, Québec, Canada).

2.4.4.5 Histological analysis

Contracted TE choroidal stromal substitutes (N=4, n=3) and TE stromas still on their anchoring paper (N=4, n=1) were fixed with 3.7% formaldehyde and embedded in paraffin. Five µm sections were stained using the Masson's trichrome stain, and observed with a Zeiss Axio Imager.Z2 microscope. The thickness of the TE stromas was measured by averaging the transversal length at multiple points throughout the stromas (> fifteen per sample) using the ImageJ software.

2.4.4.6 Uniaxial tensile tests

The mechanical properties of the TE stromas were investigated by uniaxial tensile testing. TE stromas (N=1, in quadruplets) were kept at 37°C until testing. Experiments were also performed on native human choroids (N=3). Dog bone-shaped samples were cut into the tissues and loaded onto a pair of grips mounted on an Instron ElectroPuls E1000

mechanical tester (Instron Corporation, Norwood, MA, USA). Samples were strained at a constant rate (0.2 mm/s) until failure. Ultimate tensile strength (UTS) and strain at failure were defined by the peak stress (force/initial sample area) and maximum deformation (elongation/initial length) withstood by the samples prior to failure. The elastic modulus was defined as the slope of the linear portion of the stress-strain curve.

2.4.5 Biocompatibility assessment of TE stromas

2.4.5.1 RPE seeding onto TE choroidal stromas

RPE cells (N=1) were seeded on top of TE choroidal stromas (N=2) and cultured for four to five weeks in DMEM supplemented with 10% FBS before analysis.

2.4.5.2 HUVEC seeding onto TE choroidal stromas

GFP-human umbilical vein endothelial cells (HUVEC; kindly provided by Dr. François A. Auger, Université Laval) were seeded on TE choroidal stromas (N=2) and cultured for ten days in a 1:1 DMEM 10% FBS:EGM-2 medium before stacking two TE stromas, and sandwiching the cells between the two layers for thirteen weeks.

2.4.5.3 CM seeding onto TE choroidal stromas

CM (N=2) were seeded on a TE stroma (N=1) and cultured for three weeks in CM medium before macroscopic and microscopic images were taken.

2.4.6 Statistical analyses

Data are reported as mean ± standard deviation (STD). "N" represents the number of populations, while "n" is the number of substitutes tested for each population.

The percentage of contraction data were analyzed by a one-way analysis of variance (ANOVA) comparing the means of the eight populations to ascertain whether there was any intervariability. We pooled choroidal values for biomechanical measures (UTS, failure strain and elastic modulus) after we performed a one-way ANOVA to determine variability. A Wilcoxon-Mann-Whitney test was used to find potential differences between TE stromas and native choroids. Statistical significance was established using a standard $P < 0.05$.

2.4.7 Results

2.4.7.1 Purity of isolated RPE and choroidal cells

To reconstruct self-assembled TE choroidal stromas, we used a "deconstruction-reconstruction" approach requiring isolation and expansion of RPE and choroidal cells with high purity, which were then used to re-assemble their tissue of origin. Cell purity was assessed by immunostainings and gene expression profiling.

2.4.7.1.1 Immunostainings with cell type-specific markers

All cell types were successfully isolated and expanded for at least three passages without loss of their phenotype. Figure 2.1 shows the morphology of the different cell types, along with their expression of cell type-specific markers. CSF (n=10) exhibited a diverse morphology (spindle or more stellate shape; Figure 2.1A) and could be passaged until at least P7. Less than 1% of CSF culture expressed the melanosome maturation marker HMB-45 (Figure 2.1M) and none expressed the endothelial-specific VE-cadherin (Figure 2.1I). CSF were all positive for K8/K18. As shown in Figure 2.1E-H, all cell types expressed the ubiquitous mesenchymal intermediate filament vimentin (100% positive). CVEC (n=5) showed a characteristic rounded shape (Figure 2.1B), while 80% of cells expressed the VE-cadherin (Figure 2.1J) and none expressed HMB-45 (Figure 2.1N). Less than 5% of cells expressed the epithelial intermediate filament K8/K18 (Figure 2.1R). Keratin staining has indeed been reported for endothelial cells [32]. CM (n=3), identifiable by their dendritic morphology (Figure 1C), were all HMB-45-positive (Figure 2.1O), while they were negative for VE-cadherin and K8/K18 (Figure 2.1K, S). RPE cell cultures, successfully established from two out of ten eyeballs, demonstrated a typical epithelioid morphology (Figure 2.1D) with positivity for K8/K18 (Figure 2.1T; 100% positive), and were negative for VE-cadherin (Figure 2.1L) and HMB-45 (Figure 2.1P). Since *in vitro* culture can promote keratin expression in stromal cells such as fibroblasts (Figure 2.1Q; 100% positive for K8/K18) [33, 34], we also compared gene expression profiles of CSF and RPE cultivated in the same conditions to exclude a contamination by the latter.

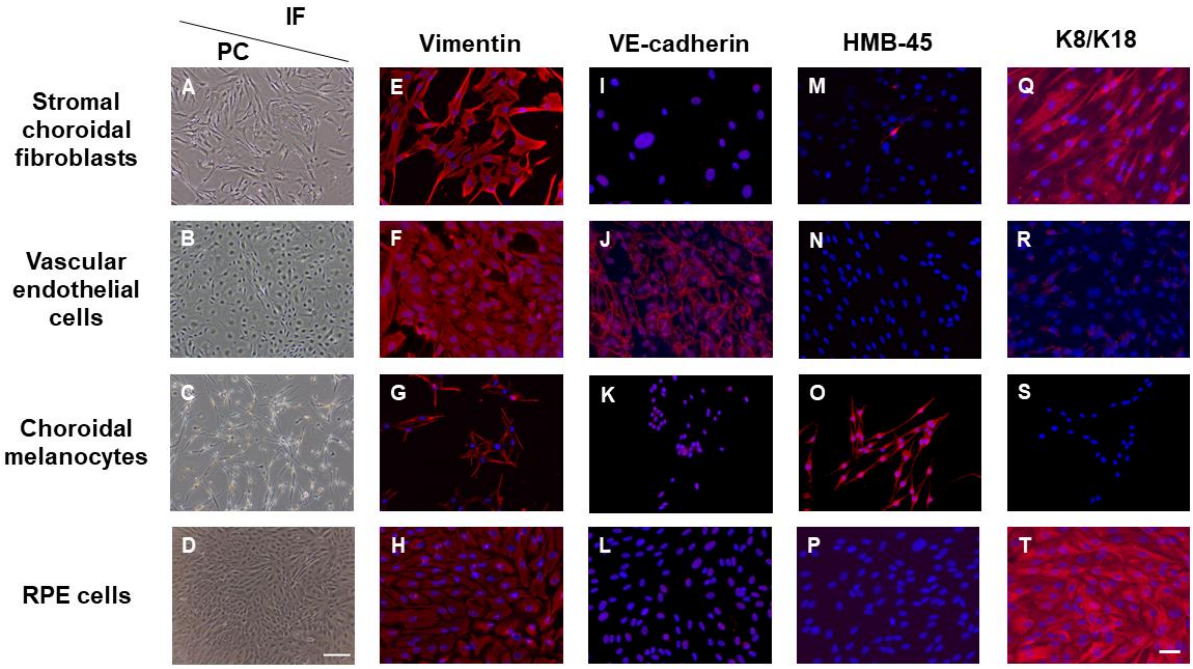

Figure 2.1 Phase contrast (PC) and immunostainings (IF) of choroidal cells and RPE. (A-D) The stromal choroidal fibroblasts, vascular endothelial cells, choroidal melanocytes and RPE cells demonstrate typical morphological characteristics as seen by PC. (E-T) Representative images of IF performed on all four cell types to verify the expression of vimentin, VE-cadherin, HMB-45 or K8/K18 (red). Cell nuclei were counterstained with Hoechst (blue). Scale bars: PC, 200 µm; IF, 50 µm.

2.4.7.1.2 Gene expression profile

The pattern of expressed genes was clearly distinctive between the CSF (combined donors) and RPE cells as shown by a scatter plot analysis of the transcripts (Figure 2.2A; R2 = 0.9312). A heatmap was also generated for the 236 transcripts showing at least a twenty-fold expression variation between the three CSF and the RPE cells (Figure 2.2B); these data confirmed that the isolated CSF were indeed pure fibroblasts.

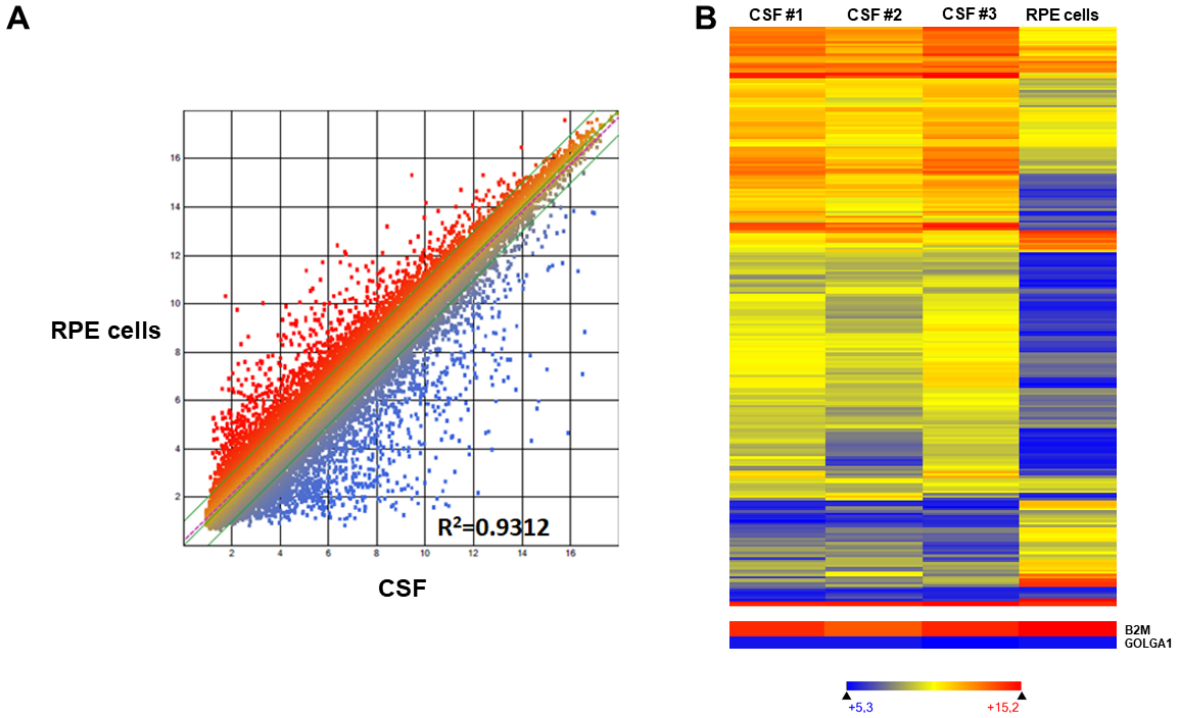

Figure 2.2 Gene expression profiling of CSF and RPE cells by microarray. (A) Scatter plot of signal intensity in log2 from 60,000 different targets covering the transcriptome of CSF (x-axis) plotted against the RPE cells (y-axis). The two-fold change in intensity lines is shown in green. The displacement of the linear regression curve (dashed purple) away from the central axis reflects the degree of divergence in the pattern of gene expression between the two cell types (R2 value, coefficient of determination). (B) Heatmap representation of transcripts differentially expressed (> twenty-fold change; 236 mRNAs) between the CSF and RPE cells. Data are also presented for the housekeeping mRNAs GOLGA1 and B2M. Transcripts indicated in dark blue correspond to those whose expression is very low, whereas highly expressed transcripts are shown in orange/red.

2.4.7.2 Tissue engineering of choroidal stromal substitutes using the self-assembly approach

Once purity of choroidal and RPE cells was confirmed, eight fibroblast populations were chosen and cultured in DMEM 10% FBS supplemented with ascorbic acid. CSF produced sheets of matrix after six weeks of culture (Figure 2.3). Two ECM sheets were stacked to form the TE choroidal stromal substitutes. These substitutes were macroscopically uniform, and could easily be manipulated without tearing.

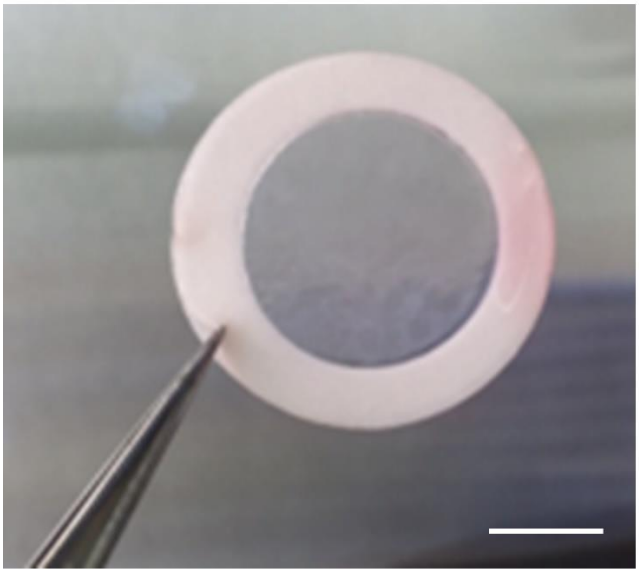

Figure 2.3 Macroscopic picture of a human TE choroidal stromal substitute. Two matrix sheets were stacked to form the substitute held by forceps on the anchoring ring. Scale bar: 1 cm.

2.4.7.3 Contractile behavior of TE choroidal stromal substitutes

2.4.7.3.1 Tissue contraction assays

Because the TE choroidal stromas contracted once released from the anchoring paper ring, we carried out contraction assays. The contraction increased sharply during the first 10 minutes (between 66 ± 1% and 88 ± 1%) before stabilizing (Figure 2.4). The TE choroidal stromas only retained less than a third of their initial size.

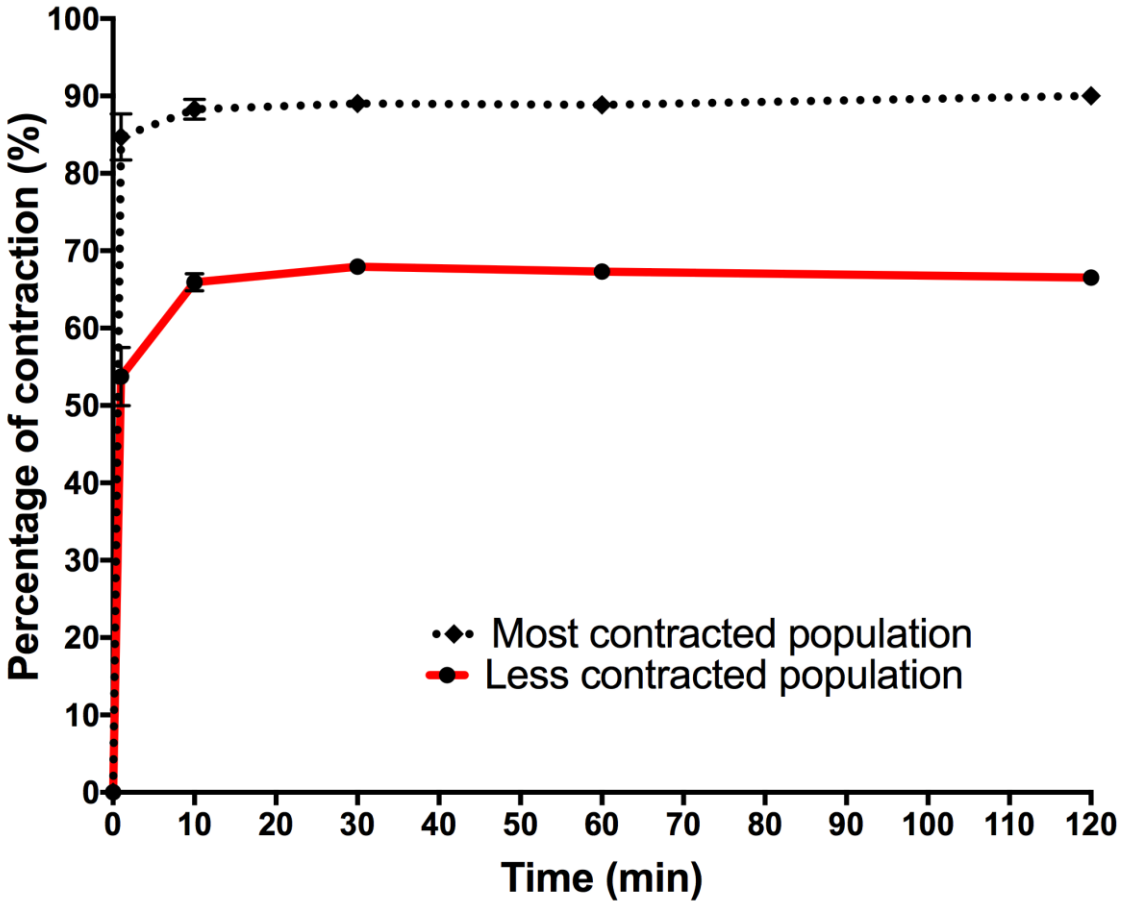

Figure 2.4 Contractile behavior of the TE choroidal stromas once released from the anchoring paper ring. Experiments were performed in triplicate using eight different cell populations; only the least and most contracted populations (percentage of contraction at 10 min: 66 ± 1% and 88 ± 1%) are shown. The remaining six populations showed a similar contraction profile. Data are presented as mean ± STD.

2.4.7.3.2 Immunostainings of contractile proteins

To explain the origin of the enhanced contractility, immunostainings of α-SMA and smoothelin were performed. Expression of α-SMA was restricted to large blood vessels in the native choroids but was found throughout the stroma in TE substitutes (Figure 2.5). Absence of smoothelin in TE choroidal stromas ruled out a contamination by smooth muscle cells, which are mostly present around blood vessels in the native choroid (Figure 2.5).

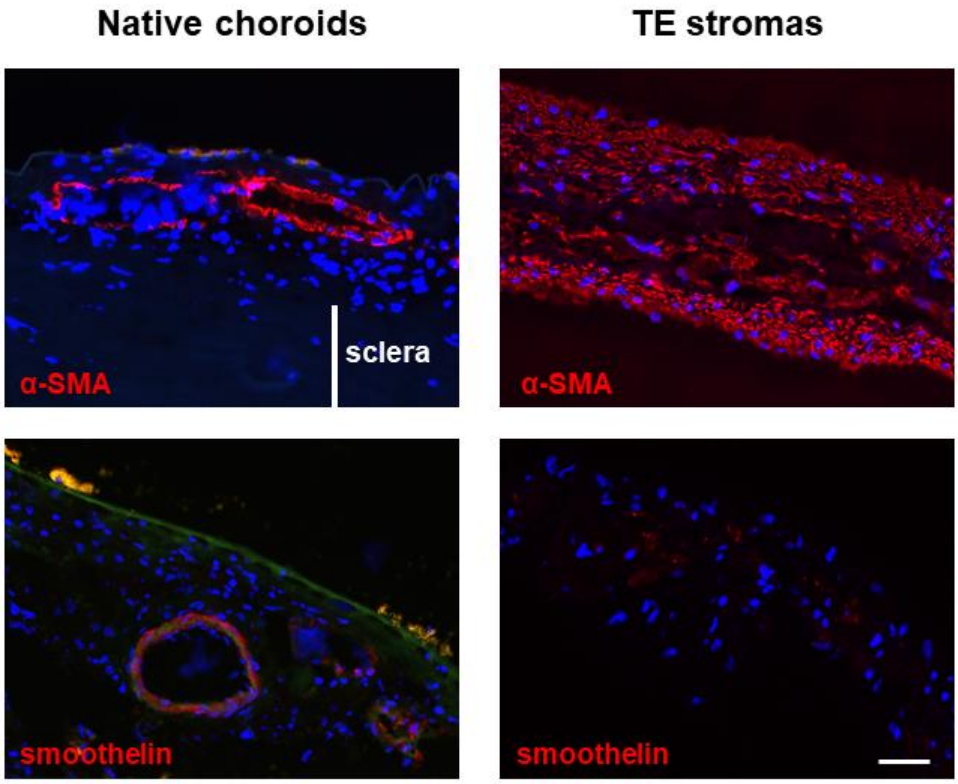

Figure 2.5 Analysis of contractile markers. Representative images of α-SMA and smoothelin immunostainings (red). Nuclei were counterstained with Hoechst (blue). The orange/yellow staining at the top of the native choroid indicates the RPE autofluorescence. TE stromas (N=8) and native choroids (N=4). Scale bar: 50 µm.

2.4.7.4 ECM composition of TE choroidal stromas

2.4.7.4.1 Mass spectrometry (MS) analysis of ECM proteins in TE choroidal stroma

Several matrix proteins were identified using MS, notably type I, III, IV, VI, VIII and XVIII collagens, which were also reported in the native choroidal stroma [35-37]. MS did not allow the detection of type V collagen normally found in the native choroidal stroma [36], probably due to the difficult digestion of this fibrillar collagen. Proteoglycans decorin, fibromodulin, lumican, perlecan and versican were also detected in the TE choroidal stroma similar to the native choroid [38]. MS analysis of native choroidal stromas was not executed, because the native tissue's composition includes elements that are not present in the TE choroidal stroma, such as Bruch's membrane, vessels and melanocytes. In order to compare the ECM protein composition of the TE choroidal stroma to its native counterpart, immunostainings were performed.

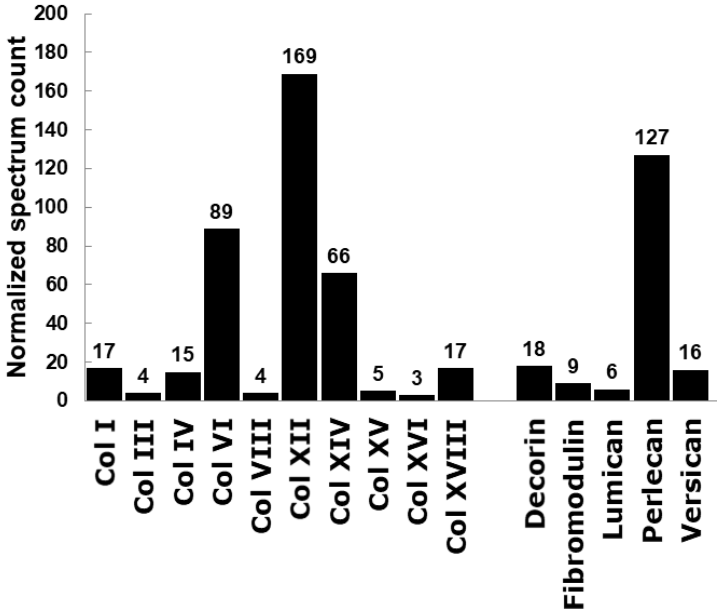

Figure 2.6 Detection of collagens (Col) and proteoglycans in the TE choroidal stroma by mass spectrometry. The value for each ECM component is expressed as the normalized spectrum count (N=1, n=1). Different proteins cannot be compared with one another.

2.4.7.4.2 Immunostainings and scanning electron microscopy (SEM) of TE choroidal stromas

To confirm the similarity in the ECM composition of both types of tissues, TE choroidal stromas and native choroids were immunostained for various matrix proteins (Figure 2.7A-B). As expected, they both expressed similar collagens (I, III, IV, V and VI) and

proteoglycans (decorin, lumican and perlecan). Two large glycoproteins absent in native choroids were detected in our TE choroidal stromas (Figure 2.7B): tenascin C (also detected by MS) and fibronectin, which participate in tissue remodeling during development or in response to injury and stress. SEM showed elongated choroidal fibroblasts embedded in ECM as expected (Figure 2.7C).

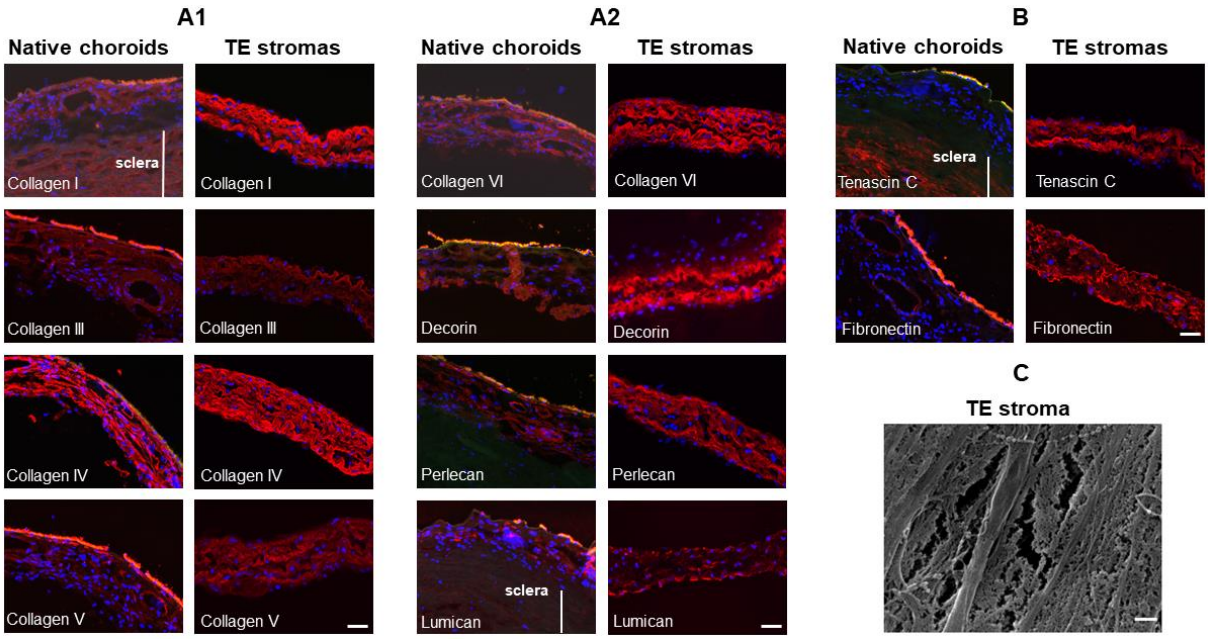

Figure 2.7 Immunostainings and SEM of contracted TE choroidal stromas. (A-B) Representative images of collagens (types I, III, IV, V and VI), proteoglycans (decorin, lumican and perlecan) and glycoproteins (tenascin C and fibronectin) (red). Nuclei were counterstained with Hoechst (blue). The orange/yellow staining at the top of some native choroids indicates the RPE autofluorescence. TE stromas (N=8) and native choroids (N=4). (C) SEM image of an anchored choroidal stroma embedded in woven collagen fibers and ECM proteins (N=3). Scale bars: A-B, 50 µm; C, 1 µm.

2.4.7.5 Thickness measurements

Masson's trichrome staining (Figure 2.8A-B) showed that the choroidal stromal substitutes were mostly comprised of ECM as seen by the uniform blue staining. Cell nuclei in purple were consistently present across the stroma. The two layers fused well together and TE choroidal stromas were rarely delaminated. Contracted stromas were four times thicker (133 ± 39 µm) than anchored stromas (30 ± 8 µm), which put them in the range of the native choroidal thickness (130.43 ± 11.82 µm; N=10).

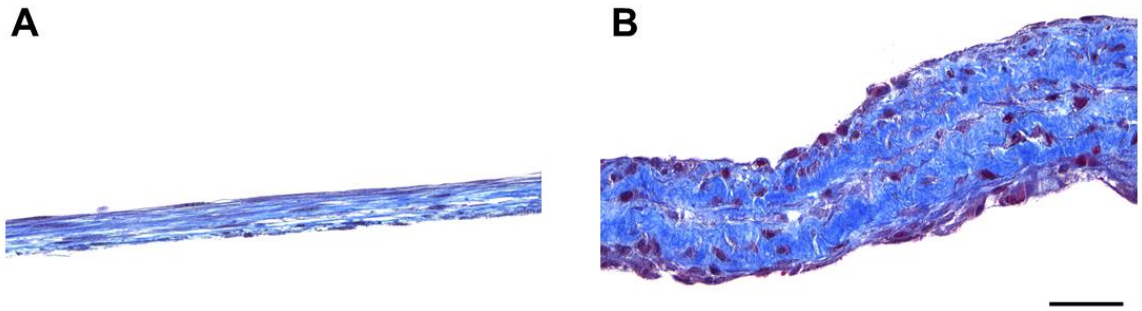

Figure 2.8 Histological cross-sections of contracted (A) and non-contracted (B) TE choroidal stromas using Masson's trichrome staining. Connective tissue appears in blue and cells in purple. Non-contracted TE choroidal stromas thickness: 30 ± 8 µm (N=4; n=1); Contracted TE choroidal stromas thickness: 133 ± 39 µm (N=4; n=3). Scale bar: 50 µm.

2.4.7.6 Mechanical parameters

Since the mechanical properties of the ECM are involved in cell behavior, tissues were submitted to tensile testing. All samples presented a stress-strain curve typical of biological tissues. TE choroidal stromas exhibited similar strain prior to failure compared to native choroids (around 30%, Figure 2.9). Ultimate tensile strength (UTS) and elastic modulus data were not significantly different ($P > 0.05$) between the two groups either, indicating that our reconstructed stromas share comparable mechanical properties with native tissues. However, mean values were higher for TE choroidal stromas suggesting that it takes more force to produce the same amount of strain.

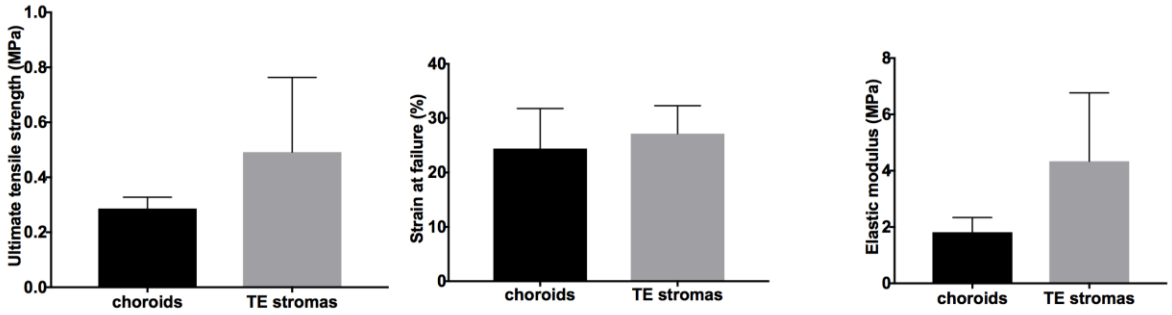

Figure 2.9 Mechanical properties of TE choroidal stromas compared to native choroids. None of the three considered parameters (UTS, strain at failure and elastic modulus) were significantly different between the two groups. One population of TE choroidal stromas was used (n=4), while 3 native choroids served as control (n=2/3). Data are presented as mean ± STD.

2.4.7.7 Growth of choroidal cells into TE choroidal stromas

RPE cells, HUVEC and CM were seeded onto TE choroidal stromas to assess the capacity of those cells to populate the reconstructed tissues in order to recreate the most representative stroma.

2.4.7.7.1 RPE seeding

RPE cells grew as a monolayer on the TE choroidal stroma as shown by the histological cross-section colored with the Masson's trichrome stain (Figure 2.10A; nuclei staining in purple on top of the blue stroma) or using the RPE autofluorescence (Figure 2.10B).

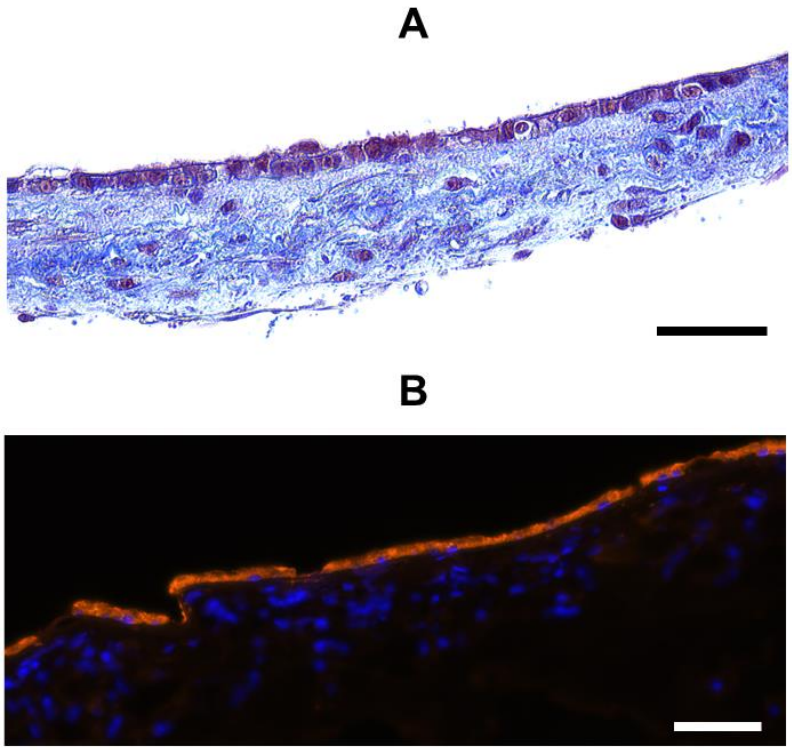

Figure 2.10 RPE cells following their seeding onto the TE choroidal stroma. (A) Histological cross-section colored with Masson's trichrome staining; cells appear in purple and connective tissue in blue. (B) The orange/yellow staining at the top of the TE stromas indicates the RPE autofluorescence. Nuclei were counterstained with Hoechst (blue). RPE cells (N=1), TE stromas (N=2). Scale bar: 50 µm.

2.4.7.7.2 HUVEC seeding

Contrary to 2D culture in which the cells grew as a monolayer (Figure 2.11A), HUVEC-GFP cells formed a vascular network in 3D culture onto the TE choroidal stroma (Figure 2.11B).

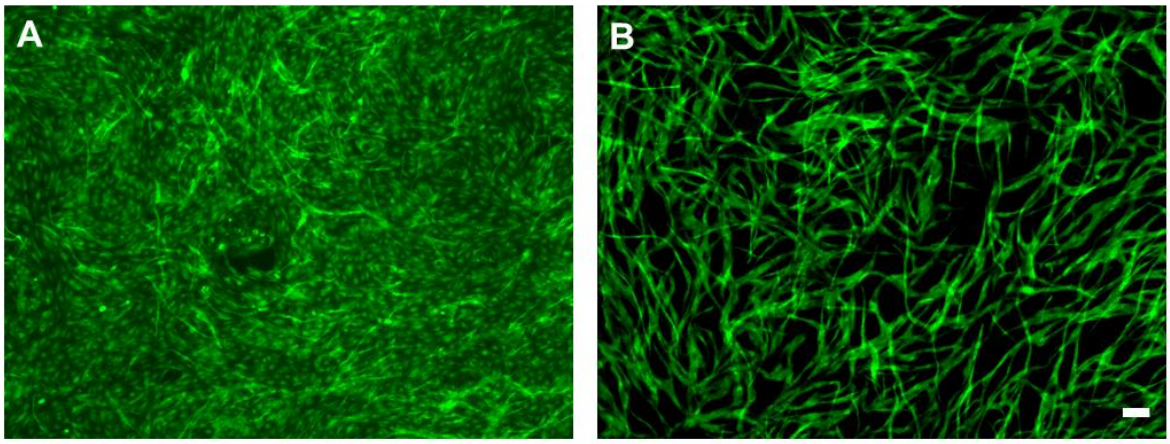

Figure 2.11 Analysis of vascularization of TE choroidal stromas. Representative images of GFP-HUVEC (green) taken ten days (A) after seeding on a TE choroidal stroma, and (B) ten weeks after sandwiching between two TE choroidal stromas (N=2). Scale bar: 100 µm.

2.4.7.7.3 CM seeding

The TE choroidal stroma became pigmented after three weeks of culture with embedded CM (Figure 2.12).

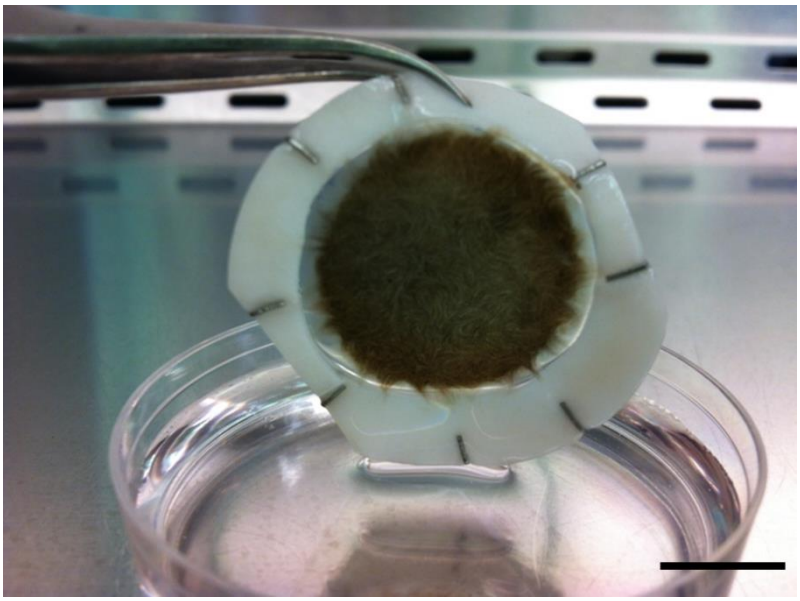

Figure 2.12 Macroscopic picture of a pigmented TE choroidal stroma. TE stroma (N=1), choroidal melanocytes (N=2). Scale bar: 1 cm.

2.4.8 Discussion

For the first time, we engineered a scaffold-free choroid by using the self-assembly approach. Reconstructed choroidal stromas had similar ECM proteins and proteoglycans composition than the native choroid. Furthermore, their biomechanical properties were akin to those of the native choroid according to the comparative measurements of ultimate tensile strength, strain and elasticity. Finally, when RPE, HUVEC and CM were seeded onto TE choroidal stromas, they repopulated the ECM and adopted a morphology and a histological appearance similar to *in vivo*.

Obtaining pure cultures of stromal fibroblasts is central to the success of tissue engineering using the self-assembly approach. Evaluation of cell purity was based on morphological, immunostaining and gene expression profiling analyses. CVEC, CM and RPE cells were all positive for vimentin as previously reported [39-42], as well as for their specific markers (VE-cadherin, HMB-45 and K8/K18, respectively). The fibroblasts purity is often determined by the expression of vimentin and the lack of staining for proteins specific to the other cells of the tissue in which they reside [42]. Our CSF indeed did not express VE-cadherin and HMB-45. However, our CSF cultures were positive for K8/K18. This result can be explained by the *in vitro* culture conditions, which have been shown to promote keratin expression in stromal cells [33, 34]. One of our concerns was the possible contamination of RPE cells within the CSF cultures since the RPE strongly adheres to the choroid. RPE cells are known to undergo epithelial-mesenchymal transition toward a fibrotic phenotype *in vitro* and to acquire some features of mesenchymal cells such as a fusiform morphology [43]. They also lose their expression of specific proteins such as RPE-65 and CRALBP (enzymes of the visual cycle) or ZO-1 (found in epithelial junctions), which could not be thus used for their identification [44]. Since K8/K18 is a retained marker of cultured RPE cells, the fact that the CSF also expressed it could lead to some ambiguity. We thus further analyzed those cultures using microarray, and the gene expression profiles of CSF and RPE cells were clearly different in the same conditions of tissue culture. Our results strongly suggest that there was no contamination of the fibroblasts cultures by RPE cells. These pure cultures were then used to form sheets of ECM using the self-assembly approach of tissue engineering.

We successfully engineered choroidal stromas in this unprecedented study. They were composed of natural ECM secreted and deposited by the fibroblasts. Mass spectrometry detected the presence of collagens and proteoglycans also found in native choroids [35-38]. Immunostainings confirmed their presence throughout the TE choroidal stromas. Mass spectrometry (normalized spectrum count) and immunostainings are both semi-quantitative methods and whether the ECM components were equally express between the native choroids and their engineered counterparts is unknown. Contrary to the native tissue, the TE choroidal stromas expressed fibronectin and tenascin C. Tenascin C is abundantly expressed during development and promotes fibroblast proliferation and migration, as well as ECM synthesis and assembly [45]. However, its expression is limited in most adult tissues only to be upregulated in areas of tissue injury. Mechanical stress is also a strong inducer of tenascin C in both embryonic and adult tissues, being chiefly expressed in tissues under high tensile stress [46], which might explain the scleral staining. Fibronectin shares similar roles in wound healing with tenascin C. It is thus not surprising to find these glycoproteins in our TE choroidal stromas. Combined with the lack of local endocrine and paracrine chemical signals found *in vivo*, our TE stromas are more likely to be representative of ECM formed during wound healing, also explaining the enhanced contractility which helps pull the wound edges together *in vivo* [47, 48].

Indeed, our TE choroidal stromas were highly contractile. In this 3D structure, the CSF expressed α-SMA. Expression of α-SMA is associated with increased cell contraction and may indicate transition of fibroblasts into a myofibroblastic phenotype. It has been shown that cells in culture display more prominent stress fibers and focal adhesions than cells *in vivo*, due to the presence of numerous growth factors in the serum and the strong adhesion to the rigid plastic substrate [47]. It thus explains the fact that TE choroidal stromas retained only at most a third of their original area once released from their anchoring paper rings. Self-contraction is quite common with the self-assembly approach; however, with careful adjustment of notably serum concentration and composition as well as culture time, sheet contraction values can drop to 0%-20% once unanchored [16, 49, 50]. It would be interesting to assess the ECM composition following longer culture times and decreased

levels of serum after stacking. Sheet contraction values indeed were reduced when a population of TE stromas was further cultured in DMEM supplemented with ascorbic acid and only 1% FBS (see supplementary data).

A potential criticism of this study is the limited access to clinical information on donors who might have had some eye diseases, including AMD. Nonetheless, macroscopic examination during dissection did not reveal any overt sign of disease. Our data were also uniform, be it with qualitative analyses (such as the presence or absence of specific ECM proteins) or with the use of more quantitative approaches (such as contraction assays and biomechanical measurements), suggesting we could derive accurate insights from this study.
Furthermore, since the choroidal matrix undergoes changes in structure with increasing age, which could potentially negatively affect the mechanical behavior [51-53] and ECM composition, it would have been interesting to use younger specimens as controls given our donors' age that ranged from 54 to 86 years.

Finally, since *in vivo*, the choroid lies under the RPE, and is composed of a vascular network, and melanocytes, we investigated its biocompatibility with RPE cells, HUVEC and CM in order to mimic the native choroid. Our results show that RPE cells seeded onto a TE choroidal stroma formed a confluent monolayer as *in vivo*. HUVEC organized into capillary-like structures when sandwiched between two TE choroidal stromas, similar to the typical organization of the vasculature *in vivo*. CM survived and synthetized melanin that gave a dark brown color to the TE stroma. Ocular melanocytes increase their pigmentary response when co-cultured with stromal and epithelial cells [54].

There have been some studies mimicking the tridimensional RPE/CC interface notably by introducing a synthetic or a biological membrane between the two cell types but, to our knowledge, no complete 3D choroid model has ever been produced [55, 56]. Further work will focus on establishing GFP-positive CVEC to trace the formation of vascular networks, since HUVEC are not the most suitable for the study of the choroidal vascularization due to significant differences in gene expression with the CVEC [57]. The next step of this

research project will be to bring together the CSF, RPE cells, CVEC and CM to recreate a more accurate RPE/choroid complex.

2.4.9 Conclusion

Choroidal fibroblasts were used for the first time to engineer human choroidal stromas. The cells were easily extracted and following a relatively short period of time allowed production of substitutes whose ECM composition as well as biomechanical properties, key features of the choroid *in vivo*, were similar to the native tissue. By recapitulating the choroidal microenvironment, TE choroidal stromas also helped RPE cells, HUVEC and melanocytes to repopulate the stroma and mimic structures similar to *in vivo* conditions. They could thus be used as study models to understand cells-ECM interactions in the choroid. They may also lead to better insight in diseases affecting the choroid such as AMD, and could be utilized in therapeutics and drug development.

2.4.10 Acknowledgments

This work was supported by the Foundation Fighting Blindness. Procurement of eyeballs for research was possible thanks to the CUO Eye Bank and a FRQ-S Vision Health Research Network Infrastructure Program. S.P. and S.L. are Research Scholars of the FRQ-S (in partnership with the "Fondation Antoine Turmel" for S.P.). A.D.D. is a recipient of a Master Training Award from the Fondation du CHU de Québec.

The authors would like to thank Karine Zaniolo, Olivier Rochette-Drouin, Noémie Goyette-Lyonnais and Marie Guimond for technical assistance, Alicia Montoni, Karine Zaniolo and Sylvain Guérin for microarray analyses, the Proteomic platform at CHU de Québec for the mass spectrometry analysis, the IBIS microscopy platform at Université Laval for the preparation of the scanning electron microscopy sample, and the Histology platform at Centre LOEX.

2.4.11 References

1. Nickla, D.L. and J. Wallman, The multifunctional choroid. Prog Retin Eye Res, 2010. 29(2): p. 144-68.

2. Blaauwgeers, H.G., et al., Polarized vascular endothelial growth factor secretion by human retinal pigment epithelium and localization of vascular endothelial growth factor

receptors on the inner choriocapillaris. Evidence for a trophic paracrine relation. Am J Pathol, 1999. 155(2): p. 421-8.

3. Bhutto, I. and G. Lutty, Understanding age-related macular degeneration (AMD): relationships between the photoreceptor/retinal pigment epithelium/Bruch's membrane/choriocapillaris complex. Mol Aspects Med, 2012. 33(4): p. 295-317.

4. Wong, W.L., et al., Global prevalence of age-related macular degeneration and disease burden projection for 2020 and 2040: a systematic review and meta-analysis. Lancet Glob Health, 2014. 2(2): p. e106-16.

5. Ambati, J. and B.J. Fowler, Mechanisms of age-related macular degeneration. Neuron, 2012. 75(1): p. 26-39.

6. Ambati, J., J.P. Atkinson, and B.D. Gelfand, Immunology of age-related macular degeneration. Nat Rev Immunol, 2013. 13(6): p. 438-51.

7. Summers, J.A., The Choroid as a Sclera Growth Regulator. Experimental eye research, 2013. 114: p. 120-127.

8. Hong, L., J.D. Simon, and T. Sarna, Melanin structure and the potential functions of uveal melanosomes. Pigment Cell Res, 2006. 19(5): p. 465-6.

9. Peters, S., et al., Melanin protects choroidal blood vessels against light toxicity. Z Naturforsch C, 2006. 61(5-6): p. 427-33.

10. Hu, D.N., J.D. Simon, and T. Sarna, Role of ocular melanin in ophthalmic physiology and pathology. Photochem Photobiol, 2008. 84(3): p. 639-44.

11. Leu, S.T., et al., Drusen are Cold Spots for Proteolysis: Expression of Matrix Metalloproteinases and Their Tissue Inhibitor Proteins in Age-related Macular Degeneration. Exp Eye Res, 2002. 74(1): p. 141-54.

12. Benedicto, I., et al., Concerted regulation of retinal pigment epithelium basement membrane and barrier function by angiocrine factors. Nature Communications, 2017. 8: p. 15374.

13. Feigl, B. and D. Hutmacher, Eyes on 3D-Current 3D Biomimetic Disease Concept Models and Potential Applications in Age-Related Macular Degeneration. Advanced Healthcare Materials, 2013. 2(7): p. 1056-1062.

14. DuFort, C.C., M.J. Paszek, and V.M. Weaver, Balancing forces: architectural control of mechanotransduction. Nature reviews. Molecular cell biology, 2011. 12(5): p. 308-319.

15. Xu, X., M.C. Farach-Carson, and X. Jia, Three-Dimensional In Vitro Tumor Models for Cancer Research and Drug Evaluation. Biotechnology advances, 2014. 32(7): p. 1256-1268.

16. Proulx, S., et al., Reconstruction of a human cornea by the self-assembly approach of tissue engineering using the three native cell types. Molecular Vision, 2010. 16: p. 2192-2201.

17. Couture, C., et al., The tissue-engineered human cornea as a model to study expression of matrix metalloproteinases during corneal wound healing. Biomaterials, 2016. 78: p. 86-101.

18. Michel, M., F.A. Auger, and L. Germain, Anchored skin equivalent cultured in vitro: A new tool for percutaneous absorption studies. In Vitro Cellular & Developmental Biology - Animal, 1993. 29(11): p. 834.

19. L'Heureux, N., et al., A completely biological tissue-engineered human blood vessel. FASEB journal : official publication of the Federation of American Societies for Experimental Biology, 1998. 12(1): p. 47.

20. Wystrychowski, W., et al., First human use of an allogeneic tissue-engineered vascular graft for hemodialysis access. Journal of Vascular Surgery, 2014. 60(5): p. 1353-1357.

21. Galbraith, T., et al., A Cell-Based Self-Assembly Approach for the Production of Human Osseous Tissues from Adipose-Derived Stromal/Stem Cells. Advanced Healthcare Materials, 2017. 6(4): p. n/a-n/a.

22. Vermette, M., et al., Production of a new tissue-engineered adipose substitute from human adipose-derived stromal cells. Biomaterials, 2007. 28(18): p. 2850-60.

23. Cattan, V., et al., Mechanical stimuli-induced urothelial differentiation in a human tissue-engineered tubular genitourinary graft. Eur Urol, 2011. 60(6): p. 1291-8.

24. Imbeault, A., et al., An endothelialized urothelial cell-seeded tubular graft for urethral replacement. Can Urol Assoc J, 2013. 7(1-2): p. E4-9.

25. Groupe de réflexion sur la recherche, c. and P. Lacolley, Biologie et pathologie du coeur et des vaisseaux. Nouv. éd ed. 2007, Paris: John Libbey Eurotext. xviii, 677 p., [16] p. de pl.

26. Lee, S., et al., Identification of novel universal housekeeping genes by statistical analysis of microarray data. J Biochem Mol Biol, 2007. 40(2): p. 226-31.

27. Brazma, A., et al., Minimum information about a microarray experiment (MIAME)-toward standards for microarray data. Nat Genet, 2001. 29(4): p. 365-71.

28. Shevchenko, A., et al., Mass spectrometric sequencing of proteins silver-stained polyacrylamide gels. Analytical chemistry, 1996. 68(5): p. 850.

29. Havlis, J., et al., Fast-response proteomics by accelerated in-gel digestion of proteins. Analytical chemistry, 2003. 75(6): p. 1300.

30. Keller, A., et al., Empirical statistical model to estimate the accuracy of peptide identifications made by MS/MS and database search. Anal Chem, 2002. 74(20): p. 5383-92.

31. Nesvizhskii, A.I., et al., A statistical model for identifying proteins by tandem mass spectrometry. Anal Chem, 2003. 75(17): p. 4646-58.

32. Miettinen, M. and J.F. Fetsch, Distribution of keratins in normal endothelial cells and a spectrum of vascular tumors: implications in tumor diagnosis. Hum Pathol, 2000. 31(9): p. 1062-7.

33. Sidney, L.E., O.D. McIntosh, and A. Hopkinson, Phenotypic Change and Induction of Cytokeratin Expression During In Vitro Culture of Corneal Stromal Cells. Invest Ophthalmol Vis Sci, 2015. 56(12): p. 7225-35.

34. von Koskull, H. and I. Virtanen, Induction of cytokeratin expression in human mesenchymal cells. J Cell Physiol, 1987. 133(2): p. 321-9.

35. Bhutto, I.A., et al., Localization of Collagen XVIII and the Endostatin Portion of Collagen XVIII in Aged Human Control Eyes and Eyes with Age-Related Macular Degeneration. Investigative Ophthalmology & Visual Science, 2004. 45(5): p. 1544-1552.

36. Marshall, G.E., A.G. Konstas, and W.R. Lee, Collagens in the aged human macular sclera. Curr Eye Res, 1993. 12(2): p. 143-53.

37. Tamura, Y., et al., Tissue distribution of type VIII collagen in human adult and fetal eyes. Investigative Ophthalmology & Visual Science, 1991. 32(9): p. 2636-2644.

38. Keenan, T.D., et al., Mapping the differential distribution of proteoglycan core proteins in the adult human retina, choroid, and sclera. Invest Ophthalmol Vis Sci, 2012. 53(12): p. 7528-38.

39. Hu, D.N., et al., Studies of human uveal melanocytes in vitro: isolation, purification and cultivation of human uveal melanocytes. Invest Ophthalmol Vis Sci, 1993. 34(7): p. 2210-9.

40. Zhu, M., J.M. Provis, and P.L. Penfold, Isolation, culture and characteristics of human foetal and adult retinal pigment epithelium. Aust N Z J Ophthalmol, 1998. 26 Suppl 1: p. S50-2.

41. Fenyves, A.M., J. Behrens, and K. Spanel-Borowski, Cultured microvascular endothelial cells (MVEC) differ in cytoskeleton, expression of cadherins and fibronectin matrix. A study under the influence of interferon-gamma. J Cell Sci, 1993. 106 (Pt 3): p. 879-90.

42. Chang, H.Y., et al., Diversity, topographic differentiation, and positional memory in human fibroblasts. Proceedings of the National Academy of Sciences of the United States of America, 2002. 99(20): p. 12877-12882.

43. Burke, J.M., et al., Phenotypic heterogeneity of retinal pigment epithelial cells in vitro and in situ. Exp Eye Res, 1996. 62(1): p. 63-73.

44. Kuznetsova, A. V., A. M. Kurinov and M. A. Aleksandrova (2014). "Cell models to study regulation of cell transformation in pathologies of retinal pigment epithelium." J Ophthalmol 2014: 801787.

45. Midwood, K.S. and G. Orend, The role of tenascin-C in tissue injury and tumorigenesis. Journal of Cell Communication and Signaling, 2009. 3(3-4): p. 287-310.

46. Halper, J. and M. Kjaer, Basic Components of Connective Tissues and Extracellular Matrix: Elastin, Fibrillin, Fibulins, Fibrinogen, Fibronectin, Laminin, Tenascins and Thrombospondins, in Progress in Heritable Soft Connective Tissue Diseases, J. Halper, Editor. 2014, Springer Netherlands: Dordrecht. p. 31-47.

47. Peterson, L. and K. Burridge, Focal adhesion and focal complexes, in Cell adhesion, M. Beckerle, Editor. 2001, Oxford University Press: New York.

48. Tschumperlin, D.J., Fibroblasts and the ground they walk on. Physiology (Bethesda), 2013. 28(6): p. 380-90.

49. Larouche, D., et al., Improved Methods to Produce Tissue-Engineered Skin Substitutes Suitable for the Permanent Closure of Full-Thickness Skin Injuries. Biores Open Access, 2016. 5(1): p. 320-329.

50. Gauvin, R., et al., Minimal contraction for tissue-engineered skin substitutes when matured at the air-liquid interface. J Tissue Eng Regen Med, 2013. 7(6): p. 452-60.

51. Ugarte, M., A.A. Hussain, and J. Marshall, An experimental study of the elastic properties of the human Bruch's membrane-choroid complex: relevance to ageing. Br J Ophthalmol, 2006. 90(5): p. 621-6.

52. Friberg, T.R. and J.W. Lace, A comparison of the elastic properties of human choroid and sclera. Exp Eye Res, 1988. 47(3): p. 429-36.

53. Chen, K., et al., Elastic properties of human posterior eye. Journal of Biomedical Materials Research Part A, 2014. 102(6): p. 2001-2007.

54. Smith-Thomas, L.C., et al., Cellular and Hormonal Regulation of Pigmentation in Human Ocular Melanocytes. Pigment Cell Research, 2001. 14(4): p. 298-309.

55. Fan, W., J.J. Zheng, and B.J. McLaughlin, An in vitro model of the back of the eye for studying retinal pigment epithelial-choroidal endothelial interactions. In Vitro Cell Dev Biol Anim, 2002. 38(4): p. 228-34.

56. Hamilton, R.D., A.J. Foss, and L. Leach, Establishment of a human in vitro model of the outer blood-retinal barrier. J Anat, 2007. 211(6): p. 707-16.

57. Browning, A.C., et al., Comparative gene expression profiling of human umbilical vein endothelial cells and ocular vascular endothelial cells. Br J Ophthalmol, 2012. 96(1): p. 128-32.

2.4.12 Supplementary data

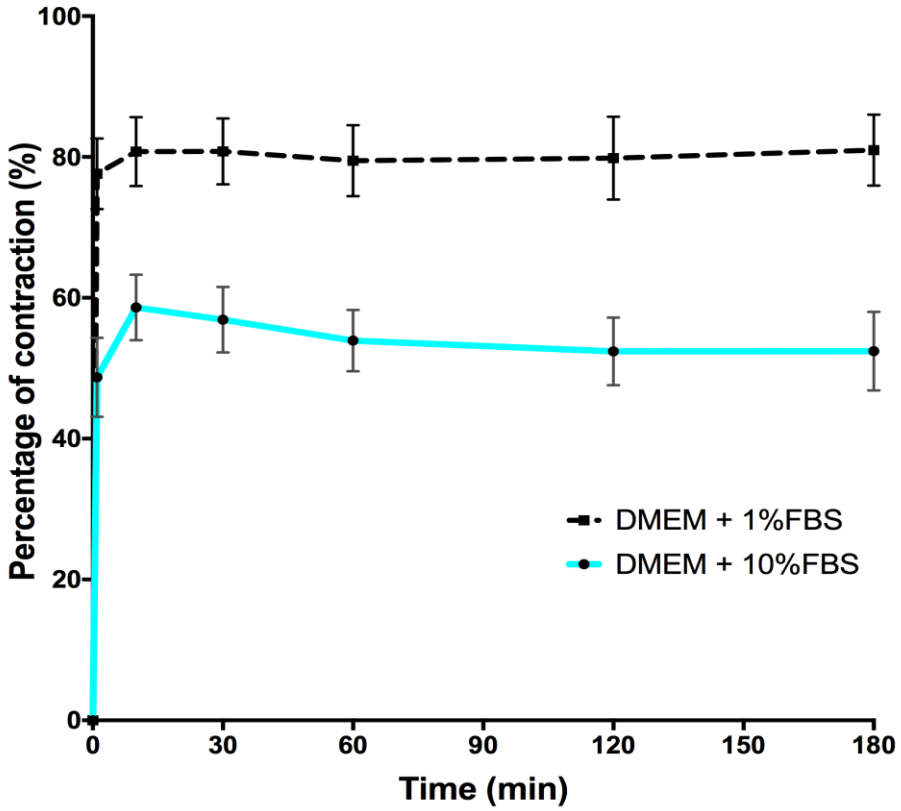

Supplementary Figure 2.1 Differential contractile behavior of a population of TE choroidal stromas following reduction of serum concentration. Experiments were performed in triplicate. Data are presented as mean ± STD.

After 7 weeks of culture in DMEM supplemented with 10% FBS and ascorbic acid once stacked, TE stromas (n=3) were cultured for an additional 12 weeks in DMEM 1% FBS and ascorbic acid. Contraction assays were then carried out (see 2.4.4.1) and results were compared to the results of the same population in triplicate (2.4.7.3.1).

Contraction values at 10 minutes dropped from 80.8 ± 4.9% to 58.6 ± 4.7% and at 3 hours from 81 ± 5.1% to 52.4 ± 5.6% indicating that reducing the percentage of serum can lower the TE stromas contractility.